Title	First-principles study on phase stability of MoSi2-NbSi2 pseudobinary alloys
Author(s)	Yuge, Koretaka; Koizumi, Yuichiro; Hagihara, Koji; Nakano, Takayoshi; Kishida, Kyosuke; Inui, Haruyuki
Citation	PHYSICAL REVIEW B (2012), 85(13)
Issue Date	2012-04
URL	http://hdl.handle.net/2433/161788
Right	©2012 American Physical Society
Type	Journal Article
Textversion	publisher

First-principles study on phase stability of $MoSi_2$-$NbSi_2$ pseudobinary alloys

Koretaka Yuge,[1] Yuichiro Koizumi,[2] Koji Hagihara,[3] Takayoshi Nakano,[4] Kyosuke Kishida,[1] and Haruyuki Inui[1]

[1]*Department of Materials Science and Engineering, Kyoto University, Sakyo, Kyoto 606-8501, Japan*

[2]*Institute for Materials Research, Tohoku University, 2-1-1 Katahira, Sendai, Miyagi 980-8577, Japan*

[3]*Department of Adaptive Machine Systems, Graduate School of Engineering, Osaka University, 2-1 Yamadaoka, Suita, Osaka 565-0871, Japan*

[4]*Division of Materials & Manufacturing Science, Graduate School of Engineering, Osaka University, 2-1 Yamadaoka, Suita, Osaka 565-0871, Japan*

(Received 16 December 2011; revised manuscript received 21 February 2012; published 16 April 2012)

The phase stability of $MoSi_2$-$NbSi_2$ pseudobinary alloys was examined by Monte Carlo simulation and the cluster expansion technique based on first-principles calculations. We found that formation energies of all possible atomic arrangements exhibited a positive sign, indicating that no stable intermediate phase exists between $MoSi_2$ with $C11_b$ and $NbSi_2$ with C40 structures. The C40 phase has significantly greater solubility as well as higher temperature dependence of solubility than $C11_b$, which agrees with previous experimental reports. Lattice vibration is found to significantly affect the solubility of both $C11_b$ and C40 phases, where its impact naturally increases at higher temperatures. From the analysis of Warren-Cowley short-range-order parameters, the $C11_b$ single phase can be interpreted as a nearly disordered state, while the C40 phase exhibits explicit deviation from the disordered state: C40 prefers Mo-Mo and Nb-Nb like-atom pairs for first-nearest-neighbor coordination, especially around equiatomic composition.

DOI: 10.1103/PhysRevB.85.134106 PACS number(s): 81.30.−t, 64.70.kd

I. INTRODUCTION

Refractory metal silicides are of great interest for superhigh-temperature structural materials, improving the performance of examples such as gas turbine engines in power generation systems. $MoSi_2$ with a $C11_b$ structure is one of the most promising candidates as a matrix phase due to its high melting temperature, low-temperature plastic deformability, low density, and outstanding oxidation resistance.[1–7] However, $MoSi_2$ exhibits poor ductility at low temperatures as well as poor creep strength at high temperatures, indicating that modification is still required for industrial applications.[8,9] $NbSi_2$ with a C40 structure has been expected to reinforce $MoSi_2$ since C40-type silicides exhibit outstanding strengthening at high temperatures compared with $MoSi_2$:[10–14] The $C11_b$/C40 duplex phase of $MoSi_2$-$NbSi_2$ pseudobinary alloys exhibits a specific lamellar structure at specific composition synthesized by zone melting and following appropriate annealing.[15,16]

Due to the fundamental importance of designing and controlling high-temperature structural materials, the thermodynamic stability of $MoSi_2$-$NbSi_2$ alloys has been addressed by several experimental works. Savitskiy *et al.*[17] predicted two-phase regions of the $C11_b$ and C40 phases at $T = 1073$ K. The phase diagram for this system was first proposed by Nakano *et al.*[18] under the assumption of a similarity in the phase diagram between $MoSi_2$-$NbSi_2$ and $MoSi_2$-$TaSi_2$ that shows a peritectic reaction.[19] They predicted that (i) the C40 phase has significantly greater solubility than $C11_b$, (ii) the peritectic point is located between $x = 0.15$ and 0.1 where x is defined as $(Mo_{(1-x)}Nb_x)Si_2$, and (iii) the $(Mo_{0.9}Nb_{0.1})Si_2$ alloy retains two-phase regions of $C11_b$ and C40 below the peritectic temperature. Subsequent experimental studies on $MoSi_2$-$NbSi_2$ alloys with a variety of composition x were performed by Wei *et al.*,[9] Nakano *et al.*,[15] Zhang *et al.*,[20] and Geng *et al.*,[21] and they supported the early prediction of the phase diagram by Nakano *et al.* Wei *et al.*[9] estimated the solubility limit using differential thermal analysis (DTA) and microstructure observation, and predicted that the solubility limit at 1673 K is around $x = 0.02$ and 0.22, which qualitatively agrees with Geng's recent study[21] of around $x = 0.04$ and 0.25. Geng *et al.*[21] showed that solubility just below the temperature of the peritectic point is around 5%. These experimental studies addressed phase stability at limited temperatures of around 1400–2000 K, and thus they lack information at low temperatures, including the possible existence of intermediate phases. Moreover, the ordering tendency on the atomic scale for $C11_b$ and C40 single phases, which quantitatively describes atomic structures in the disordered state, has not been addressed so far.

In order to quantitatively determine the phase stability of $MoSi_2$-$NbSi_2$ pseudobinary alloys over a wide range of temperatures, a theoretical approach was also performed recently: Geng *et al.*[22] employed empirical calculations using the CALPHAD (CALculation of PHAse Diagram) technique[23] based on experimental data to construct the phase diagram, which qualitatively agrees with their earlier experimental results. In their study, free energy is described as the sum of configuration entropy with the BW approximation and enthalpy as a function of composition and parameterized interaction; however, since the BW approximation typically overestimates configuration entropy and enthalpy is described by an assumed form of function, the resultant phase diagram should require further confirmation. The previous thermodynamic assessment does not address information about possible intermediate phases and atomic ordering tendencies. In order to proceed further with quantitative discussion about the phase stability of $MoSi_2$-$NbSi_2$ alloys, first-principles calculations requiring no empirical data can be naturally introduced. However, previous first-principles studies have focused on electronic structures and their related properties in $MoSi_2$ or $NbSi_2$,[24,25] and no quantitative study on phase stability has been performed so far.

In the present study, we employed first-principles calculations combined with the cluster expansion (CE) technique[26,27] and Monte Carlo (MC) statistical simulation to quantitatively investigate the phase stability of $MoSi_2$-$NbSi_2$ pseudobinary alloys with the composition of $(Mo_{(1-x)}Nb_x)Si_2$ ($0 \leqslant x \leqslant 1$). In addition to the electronic contribution to free energy, lattice vibrational contribution, which can play significant roles in the phase stability of alloys,[28–31] is also included within harmonic approximation. We discuss the possibility of intermediate phases, the solubility of $C11_b$ and C40 phases, and atomic ordering tendencies at finite temperatures.

II. METHODOLOGY

We employed the CE technique to express the configurational energy of $MoSi_2$-$NbSi_2$ pseudobinary alloys in terms of their composition and atomic arrangements. Since we used two structures $C11_b$ and C40, the CE Hamiltonian was constructed for individual structures. We considered the Helmholtz free energy of a system with given atomic arrangement $\vec{\sigma}$ at temperature T, described as

$$F(\vec{\sigma},T) = E_{\rm el}(\vec{\sigma}) + F_{\rm vib}(\vec{\sigma},T), \tag{1}$$

where $E_{\rm el}$ and $F_{\rm vib}$ denote the contribution from the electronic internal energy and vibrational free energy to the total free energy F. Note that the contribution from configuration entropy is not included in Eq. (1), and the configuration entropy is automatically included through the MC simulation described later. The details of the present CE approach are essentially the same as described in our previous papers:[32–34] Two basis functions of σ and 1 (unity) at each lattice point were used to construct complete and orthonormal basis functions, where the spin variable of $\sigma_i = +1$ (-1) represents Mo (Nb) occupation at metal site i on the $C11_b$ or C40 structure. Temperature-dependent free energies F in Eq. (1) on $C11_b$ and C40 are respectively described by

$$\begin{aligned} F_{\rm C11_b}(\vec{\sigma},T) &= \sum_{\alpha} V_{\alpha}^{\rm C11_b}(T)\Phi_{\alpha}(\vec{\sigma}), \\ F_{\rm C40}(\vec{\sigma},T) &= \sum_{\beta} V_{\beta}^{\rm C40}(T)\Phi_{\beta}(\vec{\sigma}), \\ \Phi_{\alpha}(\vec{\sigma}) &= \left\langle \prod_{i\in\alpha}\sigma_i \right\rangle, \quad \Phi_{\beta}(\vec{\sigma}) = \left\langle \prod_{p\in\beta}\sigma_p \right\rangle, \end{aligned} \tag{2}$$

where Φ_α and Φ_β are expansion functions and are called cluster functions, and $V_\alpha^{\rm C11_b}$ and $V_\beta^{\rm C40}$ are expansion coefficients and are called effective cluster interactions (ECIs) on the $C11_b$ and C40 structures, respectively. The ECIs include contributions from electronic internal and vibrational free energy as described in Eq. (1), which therefore depend on temperature. The summations were taken over possible symmetry-nonequivalent clusters α or β, and the product of spin variables was taken over lattice points composed of cluster α or β. Brackets $\langle\ \rangle$ denote the average over all possible clusters that are symmetry-equivalent to cluster α or β.

We employed first-principles calculations using a DFT code, the Vienna *ab initio* Simulation Package (VASP)[35,36] based on the projector augmented wave method,[37,38] to obtain total energies for ordered structures that are least-squares fitted to the CE Hamiltonian for the $C11_b$ and C40 structures in Eq. (2) to determine the ECIs. The ordered structures consisted of 58 and 50 structures on $C11_b$ and C40 with up to 48 atoms, respectively. The generalized gradient approximation Perdew-Burke-Ernzerhof (GGA-PBE)[39] was employed to treat the exchange-correlation functional. A plane-wave cutoff energy of 400 eV was used throughout the calculations. Geometry optimization was performed until the residual forces became less than 1 meV/Å. Brillouin-zone integration was performed on the basis of the Monkhorst-Pack scheme[40] with a $8 \times 8 \times 4$ k-point mesh in terms of unit cells of the $C11_b$ and C40 structures. The contribution of lattice vibration $F_{\rm vib}$ was treated within the harmonic approximation. A dynamical matrix was constructed by applying finite displacement of 0.02 Å to atoms in equilibrium positions. Note that we neglect anharmonic lattice vibrational effects, which could not be negligible at high temperature near melting points; estimation of the anharmonicity is out of our present scope. Other calculation treatments for the lattice vibration are described in detail in our previous papers.[32,34] Since there is a limitation on the number of DFT input energies, finite numbers of clusters that are optimal for describing the system of interests should be selected. Details of how to select clusters and structures are described in our previous papers:[33,34,41] In brief, we employed a genetic algorithm[42,43] in order to minimize the uncertainty of energies predicted by the ECIs, which is called a cross-validation (CV) score.[44–47] DFT input structures are chosen by including an initial set of randomly selected structures and lower- and higher-energy structures for each composition iteratively obtained by the CE.

We applied ECIs for the optimal set of clusters to MC simulation under a semi-grand-canonical ensemble based on the Metropolis algorithm[48] to obtain the relationship between composition x and the difference in chemical potential, which was used to construct the phase diagram. It was found to be sufficient for the cell-size dependence of the MC results to use a cell of $12 \times 12 \times 12$ expansion of $C11_b$ and C40 unit cells under three-dimensional periodic boundary conditions. In order to assess ground-state structures at $T = 0$ K, a simulated annealing algorithm[49,50] under a canonical ensemble was employed. Starting at 3500 K, the temperature of the MC simulation box was subsequently decreased by 20 K after 3000 MC steps per site. At finite temperatures, 10 000 MC steps per site were performed for equilibration, followed by 8000 MC steps per atom for sampling at each temperature and composition. In each MC step, the total energies of the system, atomic position, and correlation functions were stored.

III. RESULTS AND DISCUSSION

Following the procedure in Sec. II, we individually chose ten clusters consisting of one empty, one point, four pair, one triplet, and three quadruplet clusters for the $C11_b$, and one empty, one point, four pair, two triplet, and two quadruplet clusters for the C40 structures. Multibody cluster figures on respective structures are shown in Fig. 1. For the electronic

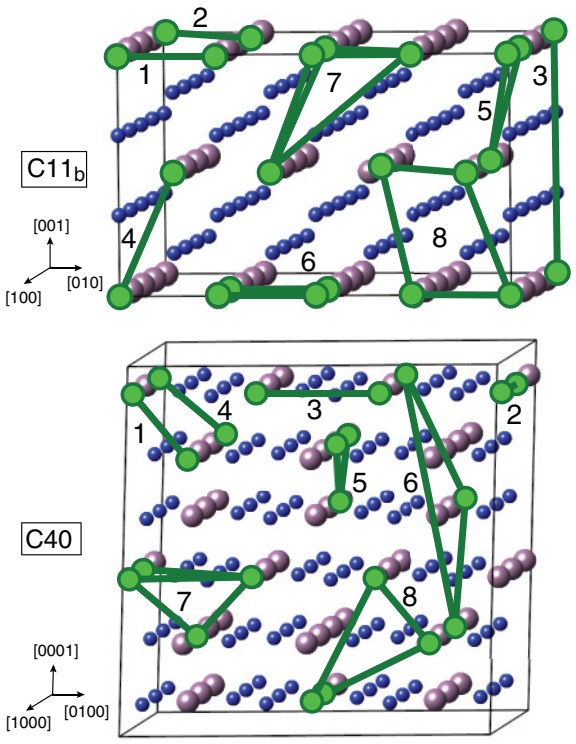

FIG. 1. (Color online) Selected multibody clusters for $C11_b$ (upper figure) and C40 (lower figure) structures. Large and small spheres are Mo (Nb) and Si sites for the $C11_b$ (C40) structure, and bold circles connected with bold lines denote clusters. Axes for conventional cells are described together.

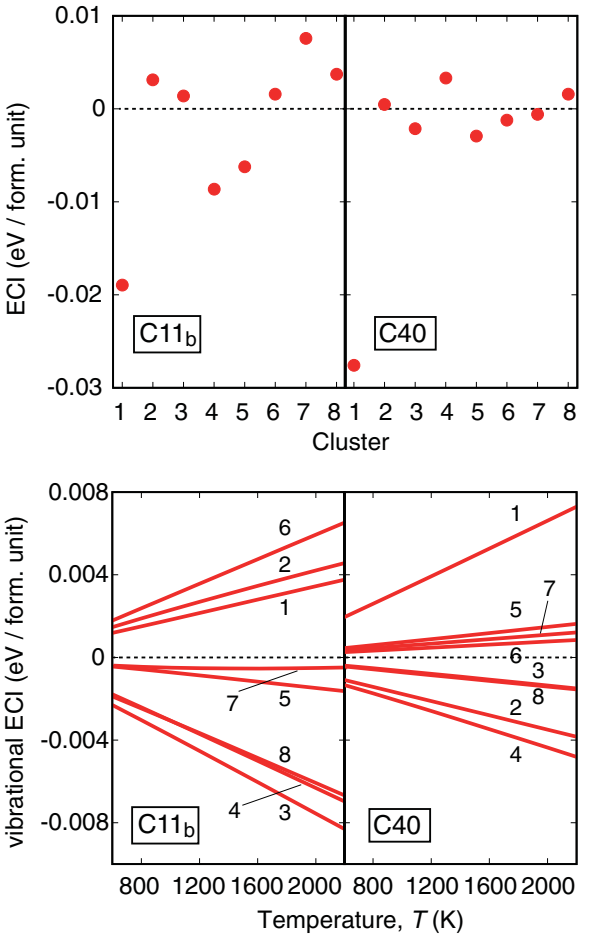

FIG. 2. (Color online) Upper figure: Electronic contribution E_{el} to ECIs of multibody clusters for $C11_b$ and C40 structures. Lower figure: Vibrational contribution F_{vib} to ECIs as a function of temperature, T.

contribution, the sets of clusters exhibited CV scores of 2 meV and 1.5 meV per formula unit where standard deviation of energies for the above 58 and 50 DFT input structures is 289 and 190 meV per formula unit for $C11_b$ and C40, respectively. These clusters gave sufficient accuracy for expressing the relative energies of individual atomic arrangements for both $C11_b$ and C40. For vibrational contribution, CV scores were $\sim 0.03 k_B T$ and $\sim 0.02 k_B T$ per formula unit for $C11_b$ and C40, which have sufficient accuracy for describing relative vibrational free energies for DFT input structures. The corresponding electronic and vibrational contributions to ECIs are shown in Fig. 2.

From the upper figure in Fig. 2, we can clearly see that the dominant contribution to total energy comes from the ECI of cluster 1, i.e., the first-nearest-neighbor (1-NN) pair for both $C11_b$ and C40. Corresponding ECIs exhibit a negative sign, indicating that $C11_b$ and C40 strongly disfavor Mo-Nb unlike-atom pairs along 1-NN coordination and would tend to undergo phase separation. From the lower figure in Fig. 2, the vibrational contribution to total energy is around one order smaller than the electronic contribution at a low temperature of $T \sim 600$ K, while it is in the same order as the electronic contribution at a high temperature of $T \sim 2200$ K. Therefore, lattice vibration should reasonably play significant roles in the phase stability of $MoSi_2$-$NbSi_2$ alloys, especially at high temperatures. For lower temperature below 600 K, the vibrational ECIs become gradually close to almost zero (but not exactly zero due to zero-point energy) at $T = 0$ K, which is in negligible order to electronic contribution to ECIs. Note that due to the nonnegligible impact of ECIs for multibody clusters other than the 1-NN pair and to difference in temperature dependence of vibrational ECIs, quantitative discussion about phase stability should require the consideration of all the electronic and vibrational ECIs, including multibody clusters.

According to the above discussion, the $MoSi_2$-$NbSi_2$ alloy is expected to undergo phase separation since the mixture of $MoSi_2$ and $NbSi_2$ would cause a positive energy gain due to the strong disfavor of the neighboring Mo-Nb unlike-atom pair. In order to quantitatively assess the stable intermediate phase, optimized ECIs on $C11_b$ and C40 are applied to MC simulation with multiple composition x. For the present pseudobinary alloy, even $4 \times 4 \times 4$ expansion of $C11_b$ and C40 unit cells has an astronomical number of possible atomic arrangements ($\sim 10^{37}$ and $\sim 10^{56}$), so estimation of the formation energies of all these arrangements is not practical. In the present work, we performed MC simulation of a 128-metal (192-metal) atom supercell with seven (eleven) compositions of x: $0.125 \leqslant x \leqslant 0.875$ with a composition grid of 0.125 ($0.083 \leqslant x \leqslant 0.916$ with a composition grid of 0.083) for the $C11_b$ (C40) structure based on the simulated annealing algorithm, as described in Sec. II. We found that the formation energy for all the possible atomic arrangements on $C11_b$ and C40 exhibited a positive sign with respect to $MoSi_2$ with $C11_b$ and $NbSi_2$ with C40

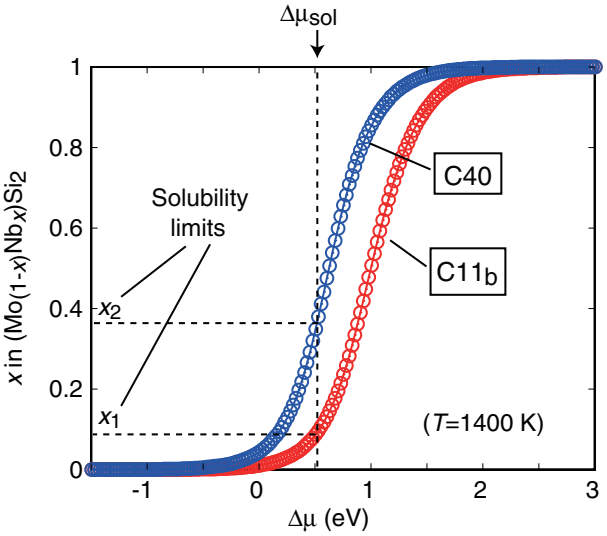

FIG. 3. (Color online) Simulated composition x at $T = 1400$ K on $C11_b$ and C40 as a function of the difference in chemical potential $\Delta\mu$. The curves for $C11_b$ and C40 are obtained by increasing and decreasing $\Delta\mu$ during the MC simulation, respectively.

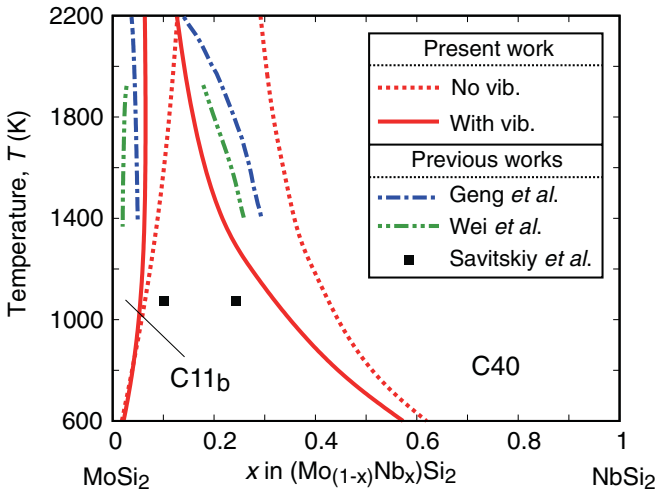

FIG. 4. (Color online) Calculated phase diagram for $MoSi_2$-$NbSi_2$ pseudobinary alloys in the composition range of $(Mo_{(1-x)}Nb_x)Si_2$ $(0 \leqslant x \leqslant 1)$. Broken and solid curves denote present calculation results without and with taking account of lattice vibrational effects. Chain curves denote theoretical prediction based on experimental thermodynamic data by Geng *et al.* (Ref. 22). Two-dot chain curves denote experimental study based on microstructural observation and DTA method by Wei *et al.* (Ref. 9). Filled squares represent experimental study of isothermal section at 800 °C by Savitskiy *et al.* (Ref. 17).

structure, indicating that no stable ground-state structures exist and thus the $MoSi_2$-$NbSi_2$ pseudobinary alloy has no stable intermediate phase.

Next, we constructed a phase diagram using the ECIs and semi-grand-canonical MC (GCMC) simulation. In order to obtain the phase boundary in the GCMC simulation, we estimated composition x as a function of $\Delta\mu = \mu_{NbSi_2} - \mu_{MoSi_2}$,[32] where μ_{MoSi_2} and μ_{NbSi_2} denote the chemical potential of $MoSi_2$ and $NbSi_2$, respectively. We performed two types of MC simulation in order to estimate the phase boundary, i.e., solubility limit: (i) We increased the chemical potential $\Delta\mu$ for $C11_b$ discretely from -1.50 to 3.00 eV by 0.025 eV and (ii) we decreased $\Delta\mu$ for C40 from 3.00 to -1.50 eV by 0.025 eV. The resultant $\Delta\mu$-x curve for electronic contribution at $T = 1400$ K is shown in Fig. 3. When $\Delta\mu$ takes a value corresponding to the two-phase region between $C11_b$ and C40, the free energy curve for $C11_b$ and C40 has a common tangent. This condition can be described by

$$\int_1^{x_2} \{\Delta\mu_{C40}(x) - \Delta\mu_{sol}\}dx - \int_0^{x1} \{\Delta\mu_{C11_b}(x) - \Delta\mu_{sol}\}dx = \Delta\mu_{sol} - \Delta\mu^0, \quad (3)$$

where $\Delta\mu_{C11_b}(x)$ and $\Delta\mu_{C40}(x)$ denote chemical potentials of $C11_b$ and C40 structures as shown by the curves in Fig. 3, $\Delta\mu_{sol}$ represents chemical potential for the two-phase region, x_1 and x_2 denote the composition for the solubility limit, and $\Delta\mu^0$ is the total energy of $NbSi_2$ with the C40 measured from that of $MoSi_2$ with the $C11_b$ structure. The solubility limit of x_1 and x_2 can be determined by finding $\Delta\mu_{sol}$, which satisfies Eq. (3). The first and second terms on the left-hand side in Eq. (3) are directly assessed by performing numerical integration for the $\Delta\mu$-x curve in Fig. 3 for a given $\Delta\mu_{sol}$. By gradually changing $\Delta\mu_{sol}$ from -1.50 to 3.00 eV with a grid of 0.001 eV, we can find the specific $\Delta\mu_{sol}$ that gives the lowest difference between left- and right-hand sides in Eq. (3). In Fig. 3, $\Delta\mu_{sol}$ satisfying Eq. (3) obtained through the above procedure is described, and the resultant solubility limits of x_1 and x_2 are also indicated. Applying this procedure to other temperatures, we can construct a phase diagram over a wide range of temperatures and whole compositions. The resultant phase diagram of the $MoSi_2$-$NbSi_2$ alloys is shown in Fig. 4. Predicted solubility limits by previous studies are illustrated together. Broken and solid curves denote solubility limits without and with taking account of the lattice vibrational effects. The predictive error of solubility limit Δx based on the optimal set of ECIs in Fig. 2 and on Eq. (3) is below around ± 0.005 for the temperature we consider in Fig. 4. The C40 phase has significantly greater solubility than the $C11_b$ phase, which agrees with previous experimental works. We can clearly see that lattice vibration plays significant roles in solubility, especially at higher temperatures, which is also expected by ECIs in Fig. 2. Lattice vibration enhances the solubility of C40, while it diminishes the solubility of the $C11_b$ phase, which cannot be simply interpreted due to complicated ECIs for multibody clusters. The predicted solubility limit including lattice vibrational effects reasonably exhibits better agreement with previous experimental works than that without lattice vibrational effects. The main difference between our theoretical results and previous works appears to be the solubility limit of the C40 phase: Geng *et al.*[22] and Wei *et al.*[9] predicted that the temperature dependence of the solubility limit of C40 exhibited a convex upward curve, while our result exhibited a convex downward curve. Extrapolating such a convex-upward solubility limit of the C40 phase to $T = 0$ K would lead to the existence of C40 phase for a finite composition range, which does not agree with

our theoretical prediction that all possible ordered structures exhibit positive formation energy with respect to $MoSi_2$ with $C11_b$ and $NbSi_2$ with C40. Meanwhile, our convex-downward solubility reasonably exhibited no solubility for either $C11_b$ or C40 phases at $T = 0$ K. Another important point in the discrepancy between Geng's[22] and our results can be attributed to the differences in how the contributions of enthalpy and entropy are treated. They employed a very simplified model of configuration entropy based on the BW approximation, which neglects the effect of atomic ordering, and of enthalpy using an assumed function of composition x and interactions. Meanwhile, in the present work, the enthalpy for a given atomic arrangement was estimated within the accuracy of the CV score (1.5–2 meV/metal-atom) using the CE technique, and the contribution of configuration entropy was automatically included with the accuracy of the fitted multibody ECIs through MC simulation, which naturally results in a more accurate estimation of the solubility limits. Our theoretical results agree with an early study of the $MoSi_2$-$NbSi_2$ phase diagram by Nakano *et al.*[18] where the alloy at $x = 0.1$ exhibited a two-phase region of $C11_b$ and C40, and the alloy at $x = 0.15$ had a single C40 phase at high temperatures while it underwent phase separation with decreased temperature. The present results are also consistent with Zhang's study[20] where $C11_b$/C40 duplex phases exist in the composition range of $x = \sim 0.05$–0.2 for $T = 1473$–1773 K.

Finally, we investigated the atomic ordering tendency of the $C11_b$ and C40 single phase at finite temperatures, which has not been reported so far. We estimated the Warren-Cowley short-range order (SRO) parameter[51] α, which can be directly obtained by statistically averaged cluster functions in MC simulations.[52] Here, $\alpha < 0$ indicates the preference of the Mo-Nb unlike-atom pairs in terms of the ideally disordered state, and $\alpha > 0$ denotes disfavor of the Mo-Nb pairs. Figure 5 shows the calculated SRO parameter α for 1-NN and 2-NN pairs as a function of composition x at $T = 1200$ and 1800 K. α for 1-NN and 2-NN reasonably became close to zero when the temperature increased due to the dominant contribution of configuration entropy at high temperatures. It can be clearly seen that α for the 2-NN pair has a value close to zero for both $T = 1200$ and 1800 K, indicating that the 2-NN coordination is nearly a disordered state for $C11_b$ and C40 phases. We confirmed that α for other pairs with a longer distance than the 2-NN pair exhibited a similar tendency to that for 2-NN. Meanwhile, α for the 1-NN pair exhibited significantly higher positive values than for 2-NN, especially for near-equiatomic compositions in the C40 phase. This finding certainly indicates that the C40 single phase is not simply interpreted as a nearly ideal disordered state, and C40 prefers Mo-Mo and Nb-Nb like-atom pairs for 1-NN coordination: This is consistent with the negative sign of the electronic contribution to ECI for 1-NN pair in Fig. 2 as well as with phase separation as shown in Fig. 4. At a smaller composition of x, α for 1-NN and 2-NN pairs are close to zero, indicating that the $C11_b$ single phase can be interpreted as a nearly ideal disordered state compared with C40.

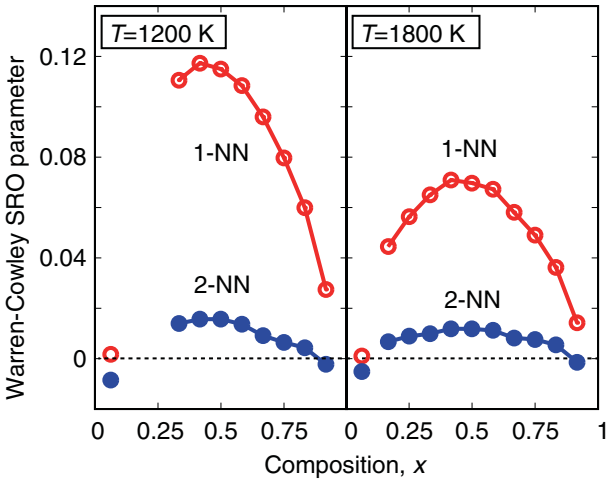

FIG. 5. (Color online) Calculated Warren-Cowley SRO parameters for 1-NN (open circles) and 2-NN (filled circles) pairs as a function of composition x. Left: $T = 1200$ K. Right: $T = 1800$ K.

IV. CONCLUSION

We employed first-principles calculations combined with the cluster expansion technique and Monte Carlo simulation to quantitatively assess the phase stability of $MoSi_2$-$NbSi_2$ pseudobinary alloys. We confirmed that no stable intermediate phase exists between $MoSi_2$ with $C11_b$ and $NbSi_2$ with C40 structures. Solubility of the C40 phase was found to be significantly higher than that of the $C11_b$ phase, which was enhanced by lattice vibrational effects, particularly at high temperatures. Predicted solubilities, including lattice vibrational effects, reasonably exhibited better agreement with previous experimental reports. Lattice vibration plays significant roles in the phase stability of $MoSi_2$-$NbSi_2$ alloys. Warren-Cowley short-range-order parameters were estimated in order to quantitatively assess the atomic ordering tendency of the $C11_b$ and C40 single phases. The $C11_b$ single phase can be interpreted as a nearly disordered state, while the C40 phase cannot be simply interpreted as a disordered state: The C40 phase prefers Mo-Mo and Nb-Nb like-atom pairs for first-nearest-neighbor pairs.

ACKNOWLEDGMENTS

This research was supported by the Advanced Low Carbon Technology Research and Development Program of the Japan Science and Technology Agency (JST).

[1] D. A. Berztiss, R. R. Berchiara, E. A. Gulbransen, F. S. Pettit, and G. H. Meier, Mater. Sci. Eng. A **155**, 165 (1992).

[2] T. Maruyama and K. Yanagihara, Mater. Sci. Eng. A **239–240**, 828 (1997).

[3] Y. Umakoshi, T. Sakagami, T. Hirano, and T. Yamane, Acta Metall. Mater. **38**, 909 (1990).

[4] S. A. Maloy, T. E. Mitchell, and A. H. Heuer, Acta Metall. Mater. **43**, 657 (1995).

[5]K. Ito, H. Inui, Y. Shirai, and M. Yamaguchi, Philos. Mag. A **72**, 1075 (1995).
[6]Y. Q. Liu, G. Shao, and P. Tsakiropoulos, Intermetallics **9**, 125 (2001).
[7]S. Lohfeld, M. Schutze, A. Bohm, V. Guther, R. Rix, and R. Scholl, Mater. Corrs. **56**, 250 (2005).
[8]J. J. Petrovic and A. K. Vasudevan, Mater. Sci. Eng. A **261**, 1 (1999).
[9]F.-G. Wei, Y. Kimura, and Y. Mishima, Mater. Trans. **42**, 1349 (2001).
[10]Y. Umakoshi, T. Nakano, E. Yanagisawa, T. Takezoe, and A. Negishi, Mater. Sci. Eng. A **239–240**, 102 (1997).
[11]T. Nakano, M. Kishimoto, D. Furuta, and Y. Umakoshi, Acta Mater. **48**, 3465 (2000).
[12]D. J. Evans, F. J. Scheltens, J. B. Woodhouse, and H. L. Fraser, Philos. Mag. A **75**, 17 (1997).
[13]H. Inui, K. Ishikawa, and M. Yamaguchi, Intermetallics **8**, 1131 (2000).
[14]H. Inui, M. Moriwaki, and M. Yamaguchi, Intermetallics **6**, 723 (1998).
[15]T. Nakano, Y. Nakai, S. Maeda, and Y. Umakoshi, Acta Mater. **50**, 1781 (2002).
[16]K. Hagihara, S. Maeda, T. Nakano, and Y. Umakoshi, Sci. Technol. Adv. Mater. **5**, 11 (2004).
[17]E. M. Savitskiy, V. V. Baron, M. I. Bychkova, S. A. Bakuta, and E. I. Gladyshevskiy, Izv. Akad. Nauk SSSR, Met. **2**, 159 (1965).
[18]T. Nakano, M. Azuma, and Y. Umakoshi, Intermetallics **6**, 715 (1998).
[19]W. J. Boettinger, J. H. Perepezko, and P. S. Frankwicz, Mater. Sci. Eng. A **155**, 33 (1992).
[20]L. T. Zhang, O. Zhu, F. Zhang, A. D. Shan, and J. S. Wu, Scr. Mater. **57**, 305 (2007).
[21]T. Geng, Ch. Li, X. Zhao, H. Xu, C. Guo, and Zh. Du, Intermetallics **18**, 1007 (2010).
[22]T. Geng, Ch. Li, X. Zhao, H. Xu, Zh. Du, and C. Guo, Calphad **34**, 363 (2010).
[23]B. Sundman, B. Jansson, and J. O. Andersson, Calphad **9**, 153 (1985).
[24]V. N. Antonov, B. Y. Yavorsky, A. P. Shpak, Vl. N. Antonov, O. Jepsen, G. Guizzetti, and F. Marabelli, Phys. Rev. B **53**, 15631 (1996).
[25]D. A. Pankhurst, Z. Yuan, D. Nguyen-Manh, M.-L. Abel, G. Shao, J. F. Watts, D. G. Pettifor, and P. Tsakiropoulos, Phys. Rev. B **71**, 075114 (2005).
[26]J. M. Sanchez, F. Ducastelle, and D. Gratias, Physica A **128**, 334 (1984).
[27]D. de Fountain, *Solid State Physics*, edited by H. Ehrenreich and D. Turnbull (Academic Press, London, 1994), Vol. 47, pp. 33–176.
[28]A. van de Walle and G. Ceder, Rev. Mod. Phys. **74**, 11 (2002).
[29]K. Yuge, A. Seko, A. Kuwabara, F. Oba, and I. Tanaka, Phys. Rev. B **74**, 174202 (2006).
[30]K. Yuge, A. Seko, I. Tanaka, and S. R. Nishitani, Phys. Rev. B **72**, 174201 (2005).
[31]V. Ozoliņš, C. Wolverton, and A. Zunger, Phys. Rev. B **58**, R5897 (1998).
[32]K. Yuge, Phys. Rev. B **79**, 144109 (2009).
[33]K. Yuge, J. Phys.: Condens. Matter **22**, 245401 (2010).
[34]K. Yuge, Phys. Rev. B **84**, 134207 (2011).
[35]G. Kresse and J. Hafner, Phys. Rev. B **47**, R558 (1993).
[36]G. Kresse and J. Furthmüller, Phys. Rev. B **54**, 11169 (1996).
[37]G. Kresse and D. Joubert, Phys. Rev. B **59**, 1758 (1999).
[38]P. E. Blöchl, Phys. Rev. B **50**, 17953 (1994).
[39]J. P. Perdew, K. Burke, and M. Ernzerhof, Phys. Rev. Lett. **77**, 3865 (1996).
[40]H. J. Monkhost and J. D. Pack, Phys. Rev. B **13**, 5188 (1976).
[41]K. Yuge, Phys. Rev. B **84**, 085451 (2011).
[42]G. L. W. Hart, V. Blum, M. J. Walorski, and A. Zunger, Nature Mater. **4**, 391 (2005).
[43]A. van de Walle, Nature Mater. **4**, 362 (2005).
[44]M. Stone, J. R. Stat. Soc. Ser. B **36**, 111 (1974).
[45]D. M. Allen, Technometrics **16**, 125 (1974).
[46]A. van de Walle, M. Asta, and G. Ceder, Calphad **26**, 539 (2002).
[47]A. van de Walle and M. Asta, Model. Sim. Mater. Sci. Eng. **10**, 521 (2002).
[48]N. Metropolis, A. W. Rosenbluth, M. N. Rosenbluth, A. H. Teller, and E. Teller, J. Chem. Phys. **21**, 1087 (1953).
[49]K. S. Kirkpatrick, C. D. Gelatt, and M. P. Vecchi, Science **220**, 671 (1983).
[50]K. S. Kirkpatrick, J. Stat. Phys. **34**, 975 (1984).
[51]J. M. Cowley, J. Appl. Phys. **21**, 24 (1950).
[52]S. Müller, J. Phys.: Condens. Matter **15**, R1429 (2003).